Neural Computing and Applications
https://doi.org/10.1007/s00521-022-07145-0

ORIGINAL ARTICLE

Recurrent neural network variants based model for Cassini-Huygens spacecraft trajectory modifications recognition

Ashraf ALDabbas[1] · Zoltan Gal[1]

Received: 12 October 2021 / Accepted: 28 February 2022

Abstract
Over the last 13.7 years period of the Cassini mission, amendments to the spacecraft's flight path were needed. This research is being carried out as there is a limited number of studies that use a temporal discrimination analysis to handle raw data. More complex inspection and analysis of the collected broad trajectory dataset is necessary to classify orbital events in the signal travel period (approximately 88 minutes on the Earth-Cassini travel channel length). This paper provides an innovative, in-depth learning method to identify offline modifications in the Cassini spacecraft trajectory. The models are based on variants of Recurrent Neural Networks (RNNs: Gated Recurrent Unit (GRU)/ Long Short-Term Memory (LSTM)/ Bidirectional Long Short-Term Memory (BiLSTM)) to derive valuable data and learn the inner data structure of the time sequence, along with the penetration of long-term and short-term phase-dependencies of the RNNs layers. To validate our models, we used a variety of statistical approaches in our analysis. A considerable number of tests have been carried out, and the findings obtained have shown that the GRU and LSTM give a substantial boost to increasing the efficiency of the detection mechanism. The proposed model would consolidate potential exploration in outer space exploration to accommodate massive databases, search for correlations, and recognize complex events and outliers with an accuracy that exceeds 99 %. This method can be utilized for similar detection processes within the future outer space expedition. The results show that binary classifications of Matthews Correlation Coefficient (MCC) are more accurate than F_1 score.

Keywords Cassini-Huygens interplanetary project · Artificial intelligence · Knowledge representation · Sensory data

1 Introduction

When evaluating and utilizing big data to get value from such vast amounts of data in contemporary complex contexts, high-quality data takes priority [1]. An event that contains several separate components or sequential occurrences, including the processing of a complex event is treated as if it's within a time limit, often as the marking of distinct, discrete occurrences within an allotted time period [2]. There are situations where the details that may be obtained to represent some method or procedure are merely an inspection of the findings; since there is an extraordinary denomination of problem in the big data framework, an extreme event must be identified [3].

In the model development process, the identification of outliers is an essential phase. The requirement to detect outliers results in the development of various outermost metrics [4]. Cassini was released from Earth in October 1997 and reached its target on July 1st, 2004 [5]. Perhaps the most important maneuver in (the whole Cassini mission) is the Saturn Orbit Insertion (SOI). It is utilized to decrease the incoming energy to a spacecraft from an interplanetary flyby and put it in a target orbit trajectory around Saturn. The flybys produced by gravity support from different planets are designed to raise spacecraft velocity substantially to the Sun, and the gravity of Saturn's largest moon Titan is also a key factor for its significant path modifications [6]. Cassini's trajectory was

✉ Ashraf ALDabbas
ashraf.dabbas@inf.unideb.hu

Zoltan Gal
gal.zoltan@inf.unideb.hu

[1] Department of Information Technology Systems and Networks, University of Debrecen, Kassai str. 26, Debrecen 4028, Hungary

Published online: 31 March 2022

set to travel away from the rings of Saturn. This fluctuation in viewing geometry resulted in several previously unseen ring kinetics and atmospheric activities, especially at Saturn's poles, being discovered for the first time. Both velocity and displacement are simple expansions of the one-dimensional formulations in two and three dimensions. For two and three-dimensional motion to be described, we must first create a set of points and an axis paradigm. When we want to find a component at point P(x, y, z) in three dimensions, we often utilize the coordinates x, y, and z to do so.

Whenever an object is traveling, the variables of x, y, and z are time-dependent functions as shown in the following: x=x(t) as illustrated in Fig. 1, y=y(t) as illustrated in Fig. 2, z=z(t) as shown in Fig. 3. The use of sampling enables us to establish inferences about distribution in time of the data. For the next six figures (1, 2, 3, 4, 5, 6) the starting and ending of the samplings are: "2004-272T06:53:22.159" and "2017-257T19:59:03.895", respectively. While sub-sample intervals appear in the bottom as a magnification with intervals "2009-123T11:53:21.788" "2009-279T19:28:09.357". Small and sometimes larger gaps in Cassini's orbit are caused by their non-periodic communication with Earth.

Within these figures, we are trying to show that spatial resolution is considered as the capacity to identify small features in a given area of space. The greater the spatial resolution, the greater the amount of detail that can be viewed.

We frequently wish to know an object's acceleration vector together with its displacement and velocity vectors across its trajectory.

Figure 4, represents the acceleration (Δv) which is an instantaneous acceleration vector. The red circle represents the average acceleration, the pace at which velocity varies is referred to as average acceleration. We may determine the average velocity over time by using the displacement.

The velocities components are shown as vectors in Fig. 5. Velocity vectors x, y, z are projected into the x–y–z–plane. The values of these velocities, components are expressed in kilometers per second. Based on our analysis, the resolution across the Cassini z-direction found to be coarse (40°), which complies with [7], and as a result, the z-component of the velocity vector in the Cassini positional frame had a considerably larger inaccuracy than y and z components of the velocity vector. A moving body's vector of velocity is always oriented tangentially to its spatial trajectory at any given time, and thus in curvilinear flight, the velocity vector direction is always varying.

When it comes to the depiction of spacecraft trajectory, it is a nuanced issue that may be tackled from a variety of perspectives. The trajectory of Cassini's interplanetary mission is shown in Fig. 6. Visualizing probe trajectory is intriguing because of the many uses it has. Many sectors, ranging from academic and public awareness goals to mission scheduling and analysis, might benefit from more investigation into this scope.

The path of the Cassini after SOI must be described as a complex compound, an inclined plane helicoid curve in the area of Saturn that travels in the Sun's own ellipse curve. Figure 7, is the illustration that shows the course of the Cassini and magnifies the last 6500 thousand samples of the mission, the start, and the ending points are pointed with red circle and cube, respectively. Due to the non-periodic correspondence between Earth and Cassini, the orbit positions of the spacecraft include tiny and sometimes greater hiatus.

As a consequence, identifying variations in the trajectory is challenging. Hiatus of the depicted helicoid trajectory can be detected due to the non-periodic sampling

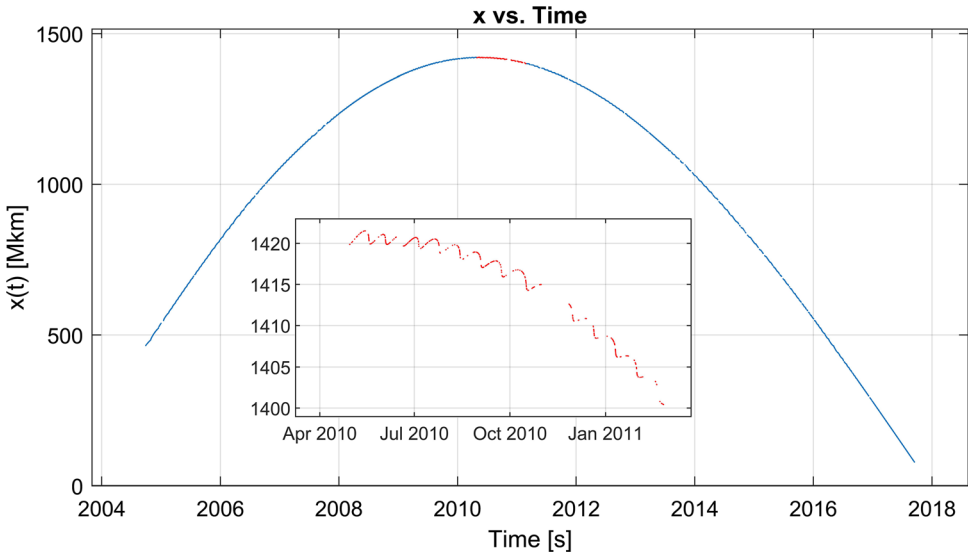

Fig. 1 Representation of Cassini's trajectory coordinate, component x as a function of time (t) in the time interval after SOI till the mission ends

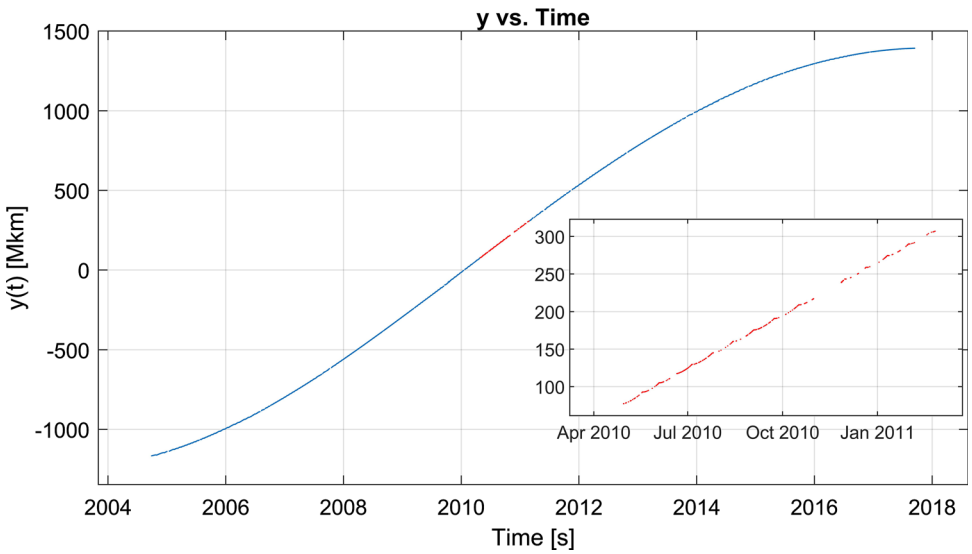

Fig. 2 Representation of Cassini's trajectory coordinate, component Y as a function of time (t) in the time interval after SOI till the mission ends

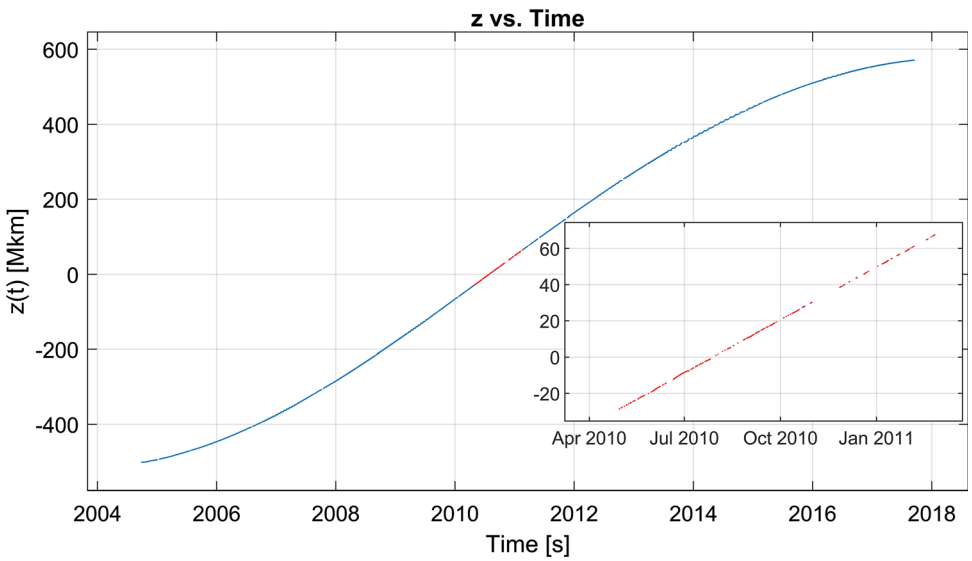

Fig. 3 Representation of Cassini's trajectory coordinate, component Z as a function of time (t) in the time interval after SOI till the mission ends

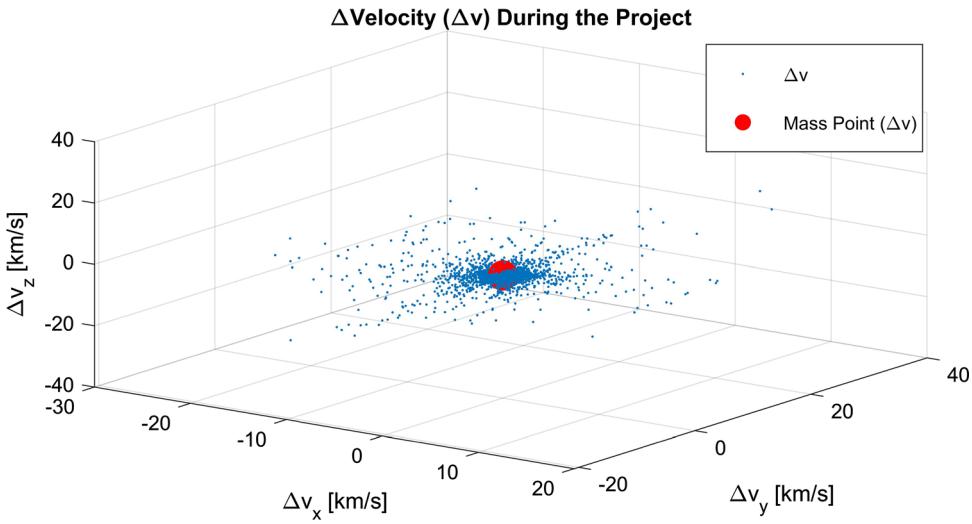

Fig. 4 Representation of Cassini velocity modification in the time interval after SOI till the mission ends

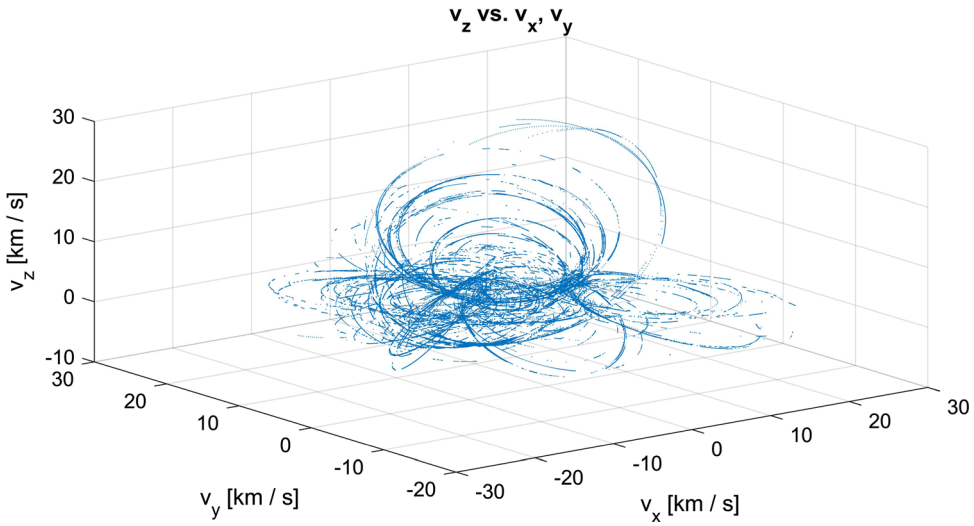

Fig. 5 Representation of Cassini velocity vectors in the time interval after SOI till the mission ends

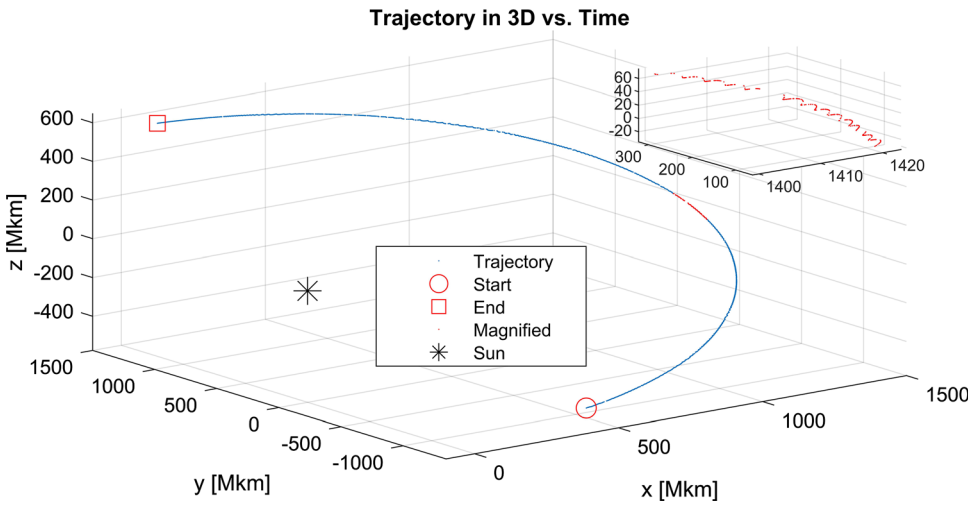

Fig. 6 Representation of Cassini's trajectory in 3D as a functions of time (t) in the time interval after SOI till the mission ends

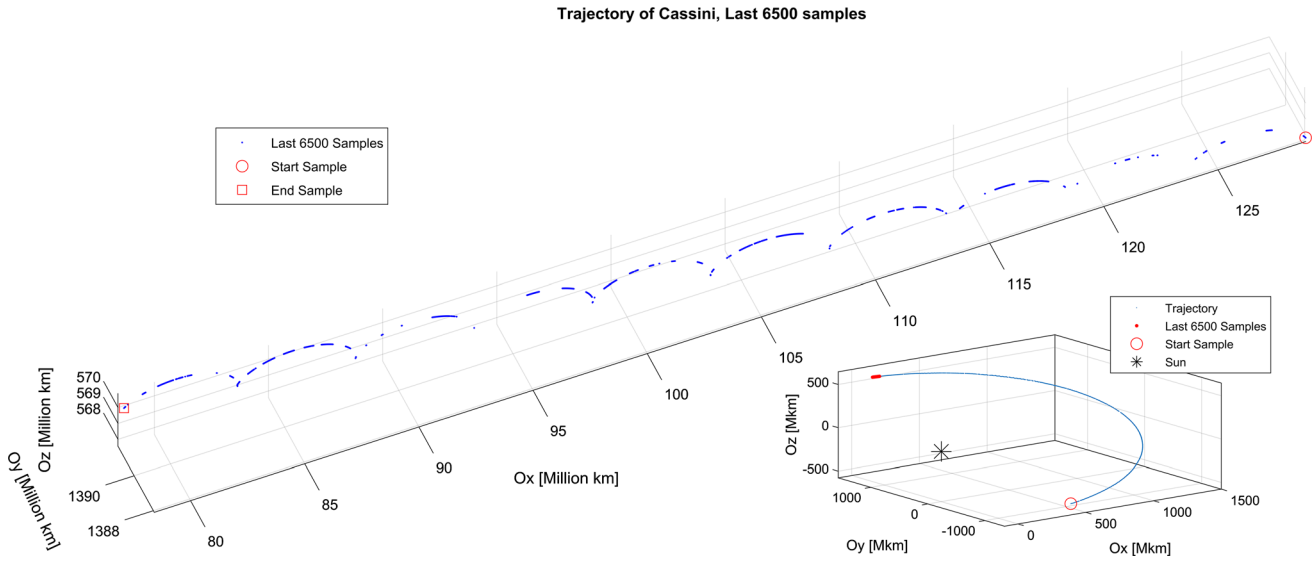

Fig. 7 Positions of the Cassini in the last 6.5 k samples (far view)

mechanism affected by the mission guidance commands coming from Earth. When we bring our approach into account, we strive to detect those modifications which occur across the Cassini orbit.

Among the main problem faced us in our research work was dealing with huge dataset was among the main issues that we had to deal with, besides how to develop a methodology to track offline events that are related to a spacecraft trajectory modifications, as there is a great distance between the Earth and the spacecraft. There were a lot of challenges regarding detecting errors in the received data packets; as around 88 minutes were needed to send or receive data between the spacecraft and the Earth via three ground stations (Deep Space Network) spread around our glop on int the United States, the second one in Spain, while the last one is in Australia, in this situation, another issue may raise, in case the same packet was received by more than one ground station, were doubled packets problem may happen. These three ground stations were needed because of the Earth rotation, to make sure that the packets are received by the station that is in the same direction as the spacecraft. The classical neural network can be applied to the problem of sequence prediction but unlike the proposed method they are stateless, which means that they learn a fixed-function approximation with a messy scaling, and fixed inputs-outputs sizes. Also, among the advantages of the provided method is its awareness of the temporal structure and contextual information, so it has the potential to impart long-term sequence correlations. RNNs maybe viewed as the architecture's incorporation of loops. For instance, inside a particular layer, each neuron may transmit its signal both (sideways) and forward to the next layer. The network's output vector may be used as an input vector for the network's next input vector.

To this end, we have placed forward our model that uses the capacity of the RNN to produce useful data and learn the deepest data structure of the time sequence, while also harnessing LSTM memory resources for pattern recognition. The remainder of this paper is structured as follows: in the next part, we include a concise literature review of some similar research in the area. The third section explains the sampling and trajectory properties of the Cassini archive) (Cassini ISS Online Data Volumes, 2020). The modification identification of spacecraft trajectory using the LSTM-based machine learning framework is discussed in Sect. 4. The procedure and experimental findings of the trajectory maneuvers identification are presented in Sect. 5. The conclusions of the study are outlined in Sect. 6.

2 Related work

There has been attention involvement in the issue on the topic of tracing spacecraft's trajectory in previous studies. Evolutionary approaches are commonly used to support the construction of spacecraft trajectories; however, principles such as Artificial Neural Networks (ANNs) and Deep Learning (DL) are still in their infancy; the explanations for the poor implementation of Machine Learning (ML) includes the shortage of readily accessible and sufficient sizeable data sets for outer space missions and the often less apparent applicability of these approaches to common problems experienced [8]. In ANN, a learning process is carried out via the use of a network structure in order to solve prediction issues [9]. This learning process is a weight set optimization issue that has motivated academics for a lengthy period of time [10]. Our study concentrates on changes in the orbiter Cassini's orbit. The trajectory within the expedition of Cassini can be divided into 3 categories of events that arise across phases. (a) launch and haulage to Saturn's orbit (b) encounter and reaching Saturn (c) and lastly, the phase of science. Launch and haulage to Saturn's orbit may allow the use of many trajectory patterns with a range of different characteristics such as a particular phase span, velocity, etc. Encounter and reaching Saturn phase will show the whole project trajectory. During the science phase, the primary purpose of trajectory layouts is to position the spacecraft in a precise location associated with Saturn that has been meticulously planned and to come up with appropriate entry parameters related to trajectory angle and velocity. In order to have elasticity in choosing the science-phase trajectory, fundamental properties of the Saturn and Cassini spacecraft have been combined. [11] has employed the method to specify the Rev-15 untapped flybys altitude of Tethys, guided by navigational conditions and operational limitations, in addition to too many route alterations, so that gross expense is kept to a minimum. [12] published a paper that examined the Cassini route, including the first and second Titan encounters. They depicted orbit determination using a complex method and the calculation of parameters relating to the descriptions of the eventual trajectory. [8] conducted a study of artificial intelligence device developments in spacecraft control and emphasized evolutionary streamlining and deep learning as the basis for potential studies. This is accomplished by drawing focus to the need to integrate artificial intelligence and computational logic into the navigation and refining of outer space flight trajectories. Until lately, previous aerospace analysis involving enormous data sets was conducted using fewer modeling-eligible strategies with immutable or temporal data as stated by the authors. In general, neural networks of this kind provide a weighted feedback

mechanism that can permit the forgetting of previously learned information and maintain the acquired knowledge.

More to the point, the built-in characteristics of LSTM (such as using streams of data and time series) are strong indicators of using extreme-event identification. Since LSTMs can account for past and current data and interconnection, they can extend the window through these options: studied or memorized weights, this was suggested by Bontemps et al. [13]. The study paper for the field's work is to examine trajectory monitoring involving interlinking measurements with effect on their different effects by using a method based on the concept of average synchronized trajectory, the aim to narrow down on the concept of the median proportional operator, as noted by Liu et al. [14]. Spilker and Edgington [15] provide the most current scientific highlights from the Cassini mission findings, according to this research, one of Titan's near flybys, which happened in the second half of 2016, altered Cassini's course, creating a sequence of twenty circles that shape fantastic orbits, which contain neighboring flybys of relatively tiny moons. Han et al. [16] include a time-triggered recurrent unit for initial step extraction, followed by training of feedback to generate the real trajectory. Silvestrini and Lavagna [17] propose a reinforcement learning approach for executing nearly necessary reconfiguration in the formation of flying spacecraft. We selected the following methodological studies provided in Table 1 as the most influential close studies in the field.

LSTM and inverse learning are utilized to deal with remodeled and predicted trajectory learning (including reinforcement learning and LSTM network, being employed to figure out collision-free routes). These positive qualities have motivated us to use RNN networks where it best serve our study goals. This study of variant types of RNN networks aims to recognize Cassini spacecraft trajectory modifications. As deep learning research papers are still limited within this field, the results of this study can be applied to a wider scope of related research. Based on the previously presented work, we can notice the importance of artificial intelligence for space exploration, such as mapping black holes, just found stars, and galaxies, and helping to chart the cosmos, has been shown, and it has also proved a game-changer when it comes to spacecraft navigating, manipulating them, as well as tracking them. It is well established that researchers may choose to undertake a technique comparison study prior to implementing their approach. At the very least, the findings should aid in the interpretation of method-comparison studies that have been published.

3 Cassini archive extraction and trajectories features

The spacecraft consisted of two distinct parts: the Huygens lander and the Cassini orbiter; Huygens detached from Cassini in 2004 to start their actual mission. Huygens went towards Titan's ambiance, Saturn planet largest moon then dropped to the farthest end down via a special kind of canopy that fills with air and allows a heavy object attached to it to descend slowly when dropped from a spacecraft, collecting samples and examining them, and sending the outcomes to the related research team further on through Cassini. The spacecraft "Cassini" was depleted of power resources after 20 years spent in the solar system. On September 15, 2017, Cassini entered Saturn's interior

Table 1 Comparison with other related work

Paper title	Proposed method	Acquired result	Dataset size	Purpose
Ref. [14]	Induced ordered aggregation operator	Improve trajectory forecasting precision	Differential GPS data	Trajectory prediction
Ref. [16]	Prediction method based on GRU	Improve forecast accuracy	Prior day's flight data	Trajectory prediction
Ref. [17]	Inverse/Reinforcement learning and LSTM	Limits lossin position accuracy	Limited dataset trajectories	Trajectory prediction
Ref. [18]	Generative adversarial networks	Non-compliant trajectories are significant	4401 flight trajectories records	To detect atypical behavior
Ref. [19]	Genetic algorithm	Stretching into solar systems	300 trajectories	Optimize trajectories
Ref. [20]	Orbit trim maneuvers performance	Determination of orbit has outpaced navigation needs	1.4 maneuvres per week on average	Orbit determination
Our proposed work	RNNs: (GRU),(LSTM) and (BiLSTM)	Accuracy that exceeds 99 %	393,976 samples	Identify offline modifications of Cassini trajectory

Table 2 The Cassini trajectory timestamps (UTC)

Event	Date	No. of orbits	Planned trajectory maneuvers	Executed trajectory maneuvers
Starting prime mission(SOI)	1 Jul 2004	75	161	112
Starting equinox mission	1 Jul 2008	64	104	70
Starting solstice mission	30 Sep 2010	155	206	141

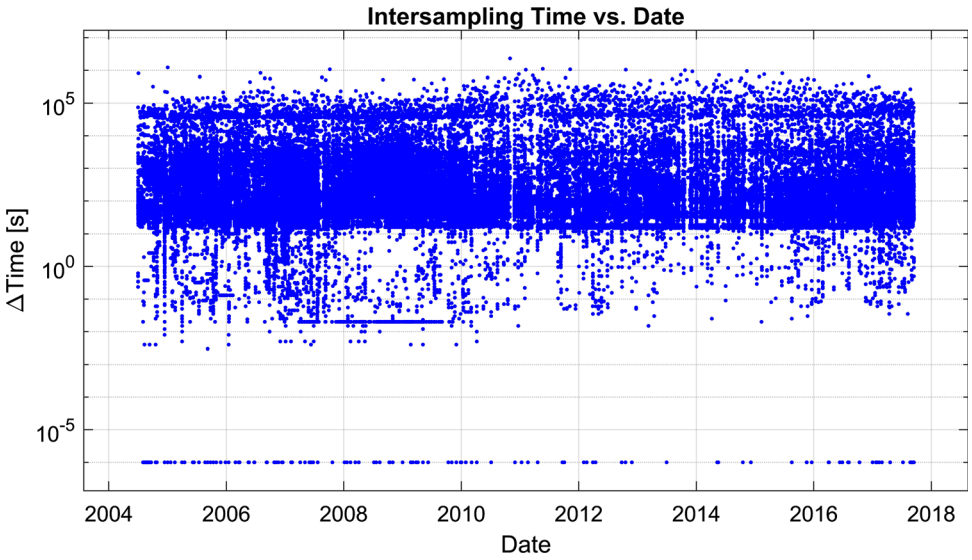

Fig. 8 Attributes of successive sampling periods of the Cassini during the analysis time interval

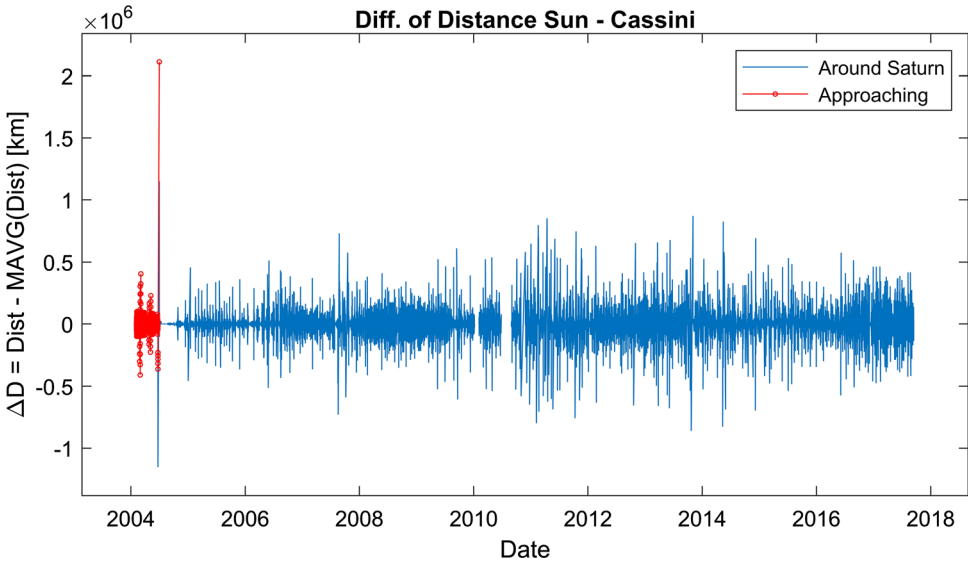

Fig. 9 Big scale distance while sampling (Sun-Cassini). Greatest distance modification was detected approximately to SOI event

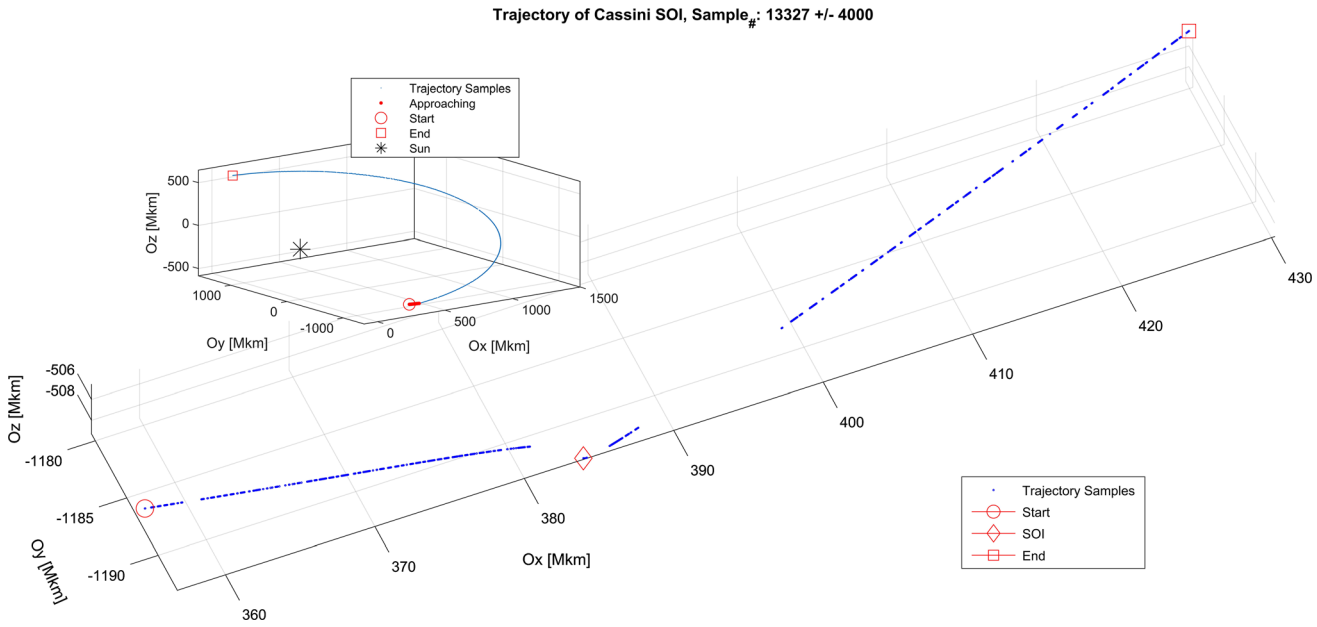

Fig. 10 Cassini's position samplings around the SOI event (closed view)

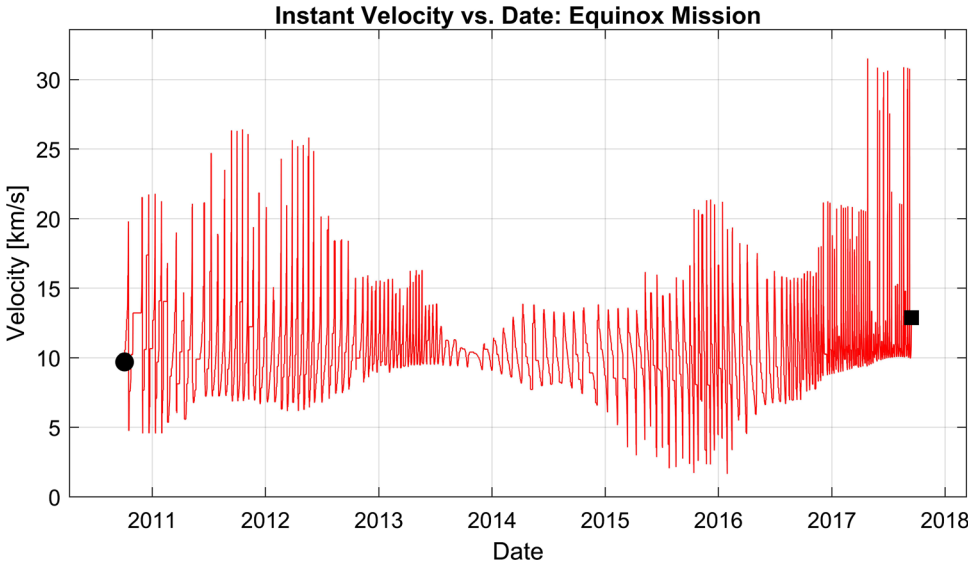

Fig. 11 Cassini spacecraft's magnitude instantaneous velocity over Equinox mission

ambiance as planned action bringing the project to a close. The Imaging Science Subsystem (ISS) produced the captured image and its related files. The ISS is made up of two separate cameras, a narrow and wide-angle. An incredibly comprehensive, interdisciplinary data collection of images and metadata for the images are accessible freely in the public domain at the image library (Cassini ISS Online Data Volumes, 2022) [21].

We have downloaded the 116 volumes from the above NASA source of the data collection analyzed by us. The beginning sample possessed a time signature of 02:07:06 on February 6, 2004, and a finishing stamp of 19:59:03 on September 14, 2017, all in Coordinated Universal Time (UTC). Table 2 summarizes the project's most significant activities. According to the mission aim, the five of the key goals of the Cassini-Huygens (C-H) project (the study of

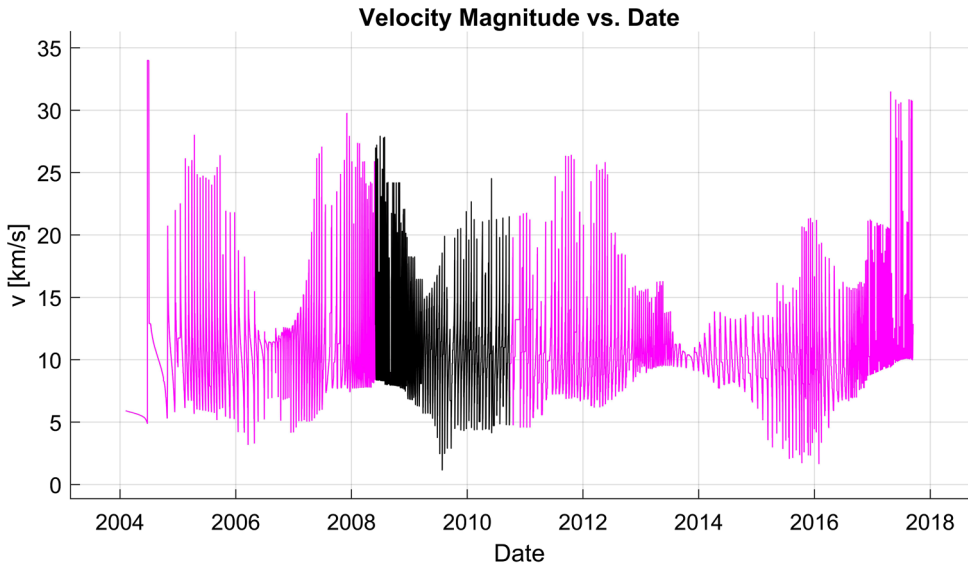

(a) velocity magnitude

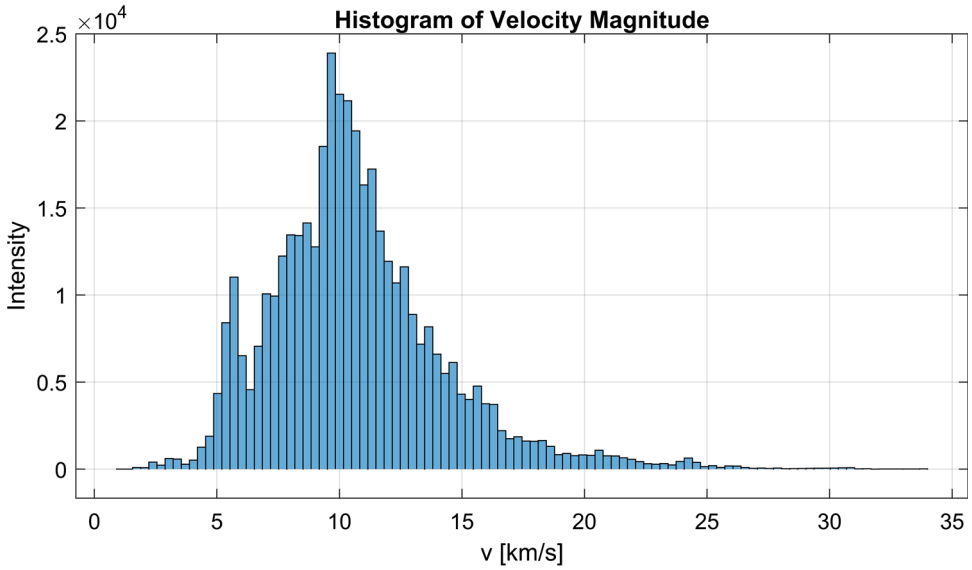

(b) histogram of velocity magnitude

Fig. 12 Attributes of Cassini's successive sampling periods

Saturn, Titan, the largest moon of Saturn, Saturn's rings, frozen asteroids, and magnetosphere) in-which could not be carried out without executing trajectory maneuvers. For each mission, the number of scheduled and performed trajectory modifications is provided by Buffington [22]. For the Prime and Equinox missions, the ratio of performed and scheduled trajectory maneuvers is 69.5 percent and 67.3 percent, sequentially. We actually lack some details of the completely performed amendments in the Solstice mission, hence our estimate of 68.4 percent (our own model is used to prepare this percentage based on past experience of two previous missions), Providing 141 modifications to the trajectory. The spacecraft data of the C-H mission, retrieved from NASA's website (Cassini ISS Online Data Volumes, 2022) [21], includes 407,303 measurements. These details cover the last 13 years and 7 months of the interplanetary mission, from February 16, 2004, to September 15, 2017. Data collection operations were conducted over a span of time, with various phases and sub-phases. Every sub-phase contains a number of sequences, each of which includes a range of observations based on the project officials' assessments. An observation is made up of a series of samplings, the scale of which is determined by the spacecraft's science events or celestial

observations surrounding Saturn. In the time frame analyzed, there were 2,355 sequences, and the number of observations was 10,851.

Figure 8 shows the features of the time difference Δt across successive samplings.

By analyzing the figure, we found out that the Δt related mean measured in seconds is 1,053 while the standard deviation is 12,282. The time prior to the insertion to Saturn orbit is represented by the red color on the left side of Fig. 9, while the phase afterward, the insertion to Saturn orbit, is represented by the blue color. The approaching process is depicted in red, while the Cassini rotation around Saturn is depicted in blue.

The Saturn Orbit Insertion (SOI) maneuver began prior to sample 13,328 of the Cassini archive, which has 116 volumes. Almost 1140 minutes are found with an absence of sampling Subsequent to the SOI event. The tiny peaks on the right-hand scale figure may also be used to detect the alteration of the distance among Sun Cassini. The SOI event is depicted in-depth in Fig. 10.

The shorter path trajectory on the distance level represents a helicoid that performs as a cross-section ellipse spectacle of the Saturnian orbit. The red circle defines the event's beginning point. At the outset of the Saturn orbit insertion, the Diamond symbol signifies the entry point (SOI) where the Cassini started orbiting the planet Saturn. In order to find out how fast the spacecraft is traveling at a certain moment, we must assess the orbiter velocity as a function of time. Our review of the NASA database yielded velocity values with respect to the solar system with the range from 3.18 to 29.75 km/s. Figure 11. reveals the pace of Cassini's velocity during the final trip phase Equinox. The interval of time between curve spikes reflects the helicoid orbiter variable time cycle. Velocity magnitude is defined by a dotted black circle and a cube shape at the start and end of each task, respectively.

In order to get the time of flight bias at a minimum, a trajectory must be plotted as a function of maneuver severity; due to that, Figure 12 is provided. We can see the spacecraft velocity magnitude and its related histogram just before the event of SOI in 2004 till the mission termination in 2017. This period includes the prime mission, the equinox mission which is highlighted with black color, and the solstice mission.

The flyby's dynamics can be adjusted in both direction and magnitude. The change in the amount of the Saturnian magnitude velocity yields a corresponding period of motion, resulting in a Cassini orbital time interval change. Cassini's angular movement is influenced by changes in the direction or magnitude of its Saturn-relative velocity, leading to a shift in spacecraft orientation. Since velocity is a vector, it is changeable in both magnitude and direction; this sentence means that it can be negative (cause to a reduction in spacecraft velocity) or positive (the spacecraft is accelerated).

4 Stipulation recognition of Cassini trajectory modification

The proposed algorithm has a robust theoretical basis and has promising experimental outcomes. We illustrate that the proposed algorithm can efficiently boost the detection process of events related to trajectory modifications on real-world data sets. The meta code of the proposed algorithm can be seen in Algorithm 1. The key task of using our learning algorithm is to determine complex events via spatial-produced data. The detection algorithm of the Cassini spacecraft trajectory modification is based on the data collected in the 116 data volumes acquired from NASA.

Algorithm 1 proposed algorithm metacode

```
[I_φ, I_a] = IdentifyExtremeEvents (x, y, z, vx, vy, vz, time, Th_φ, Th_a, N)
I_φ = ∅, I_φ = ∅
   for i = 1:N-1
      Calc. angle φ_i between consecutive velocity vectors
      Calc. magnitude of acceleration a_i
      emphif φ_i > Th_φ, then I_φ := I_φ ∪ {i}
      if a_i > Th_a then I_a := I_a ∪ {i}
   endfor # End of IdentityExtremeEvents

I = ClassifyIndexes (N, I_φ, I_a)
   I[1 : N] = False
   I[I_φ] = True
   I[I_a] = True
   RNN[1:18] = GenerateRNN (layers, MiniBatchSizes,HiddenUnits)
   RNN[1:6] = LSTM(MiniBatchSizes, HiddenUnits)
   RNN[7:12] = BiLSTM(MiniBatchSizes, HiddenUnits)
   RNN[13:18] = GRU(MiniBatchSizes, HiddenUnits)
# End of ClassifyIndexes

[LearningTime,Detection_Accuracy,MCC,F1]=TestClassification(RNN[1:18])
   RNN[1:6] = LSTM(MiniBatchSizes, HiddenUnits)
   RNN[7:12] = BiLSTM(MiniBatchSizes, HiddenUnits)
   RNN[13:18] = GRU(MiniBatchSizes, HiddenUnits)
# End of TestClassification

function GeneratePlots(LearningTime, DetectionAccuracy, MCC, F1)
   plot(LearningTime) # Learning Time of RNNs
   plot(DetectionAccuracy) # Detection Accuracy of RNNs
   plot(MCC) #Mathew Correlation Coefficient
   plot(F1) # Metric F1
# End of GeneratePlots

main ()
   [I_φ, I_a] = IdentifyExtremeEvents(...)
   I = ClassifyIndexes(...)
   RNN[1:18] = GenerateRNN(...)
   [LearningTime,Detection_Accuracy,MCC,F1] =TestClassification(...)
# End main
```

After interpretation of N = 393,977 uneven sampled records of 80 variables filtering the raw data and selecting the necessary coordinate and velocity values were executed. Based on the complex event detection explained in the next part, there were classified sampling indexes in two binary classes in function of belonging to trajectory modification events or not. First half (N/2) of the selected coordinate and velocity variables time series were used to teach three different recursive neural networks (LSTM – Long Short-Term Memory, BiLSTM – Bidirectional Long Short-Term Memory, GRU – Gated Recurrent Unit) to execute similar binary classification as the labeling method proposed by us. The third and fourth quarter of samples (N/4) were used for validation and testing classification of the samplings, respectively. Most significantly, the algorithm is capable of delivering remarkable level of accuracy based on relatively low amount of computation capacity, which justifies the virtue of the method applied. To recognize temporal interpretation for complex event detection, we increased the sensory data's time index at the time of

observation sequences, possible complex events inside the data trove may be occurring. Significantly if the Cassini spacecraft velocity vector exceeds the metric defined threshold, then it is deemed as a trajectory modification. Since velocity is a measured variable, an extreme occurrence in the trajectory means satisfying either of two conditions: a change in the direction of the velocity or a change in the acceleration vector magnitude.

4.1 Velocity vector direction modification

The angle modification velocity $\Delta\phi_i$ among successive velocity vectors v_i and v_{i+1} is provided utilizing the subsequent formula:

$$\frac{\Delta\phi_i}{\Delta t_i} = \frac{\operatorname{acos}\left(\frac{\overline{v_{i+1}}\cdot\overline{v_i}}{\|\overline{v_i}\|\cdot\|\overline{v_{i+1}}\|}\right)}{t_{i+1}-t_i}, \qquad i = 1, 2, \cdots, N-1 \tag{1}$$

where $\overline{v_i}$ and $\overline{v_{i+1}}$ are two successive Cassini vectors of velocity, $\|\overline{v_i}\|$ is the vector magnitude, Δt_i is the time period among two successive samplings and $i = 1,\ 2, \ldots, N-1$. The vectors value is the overall samples number in the Solstice, Equinox, and Prime missions: $N = 407,303 - \ 13,326 = \ 393,977$. The analyzed data represents the last 13.7 years of the C-H mission archive. Any value close to 0 indicates a very slight change of orientation per time unit ($\frac{\Delta\phi}{\Delta t}$). At the start of the mission, several of the type previously mentioned examples were found (check Fig. 13, we can see it on the values prior to 2005). With the beginning of the SOI Process, the velocity direction among the successive samplings was changing at a higher rate.

The spacecraft's trajectory was changed many times, but no accurate details regarding these incidents are currently accessible. The NASA archive, which has 116 volumes, includes samplings with a broad period dispersion. In the case of a comparatively small delay period between successive samplings, values of the $\Delta\phi/\Delta t$ by the range of over 1 rad/sec were observed.

For the most part, the movement's path varies just in a narrow range, although there are moments where the movement's direction changes significantly.

4.2 Modification of the magnitude of the acceleration vector

If the velocity vector magnitude v $(v_x,\ v_y,\ v_z)$ changes by a higher value than the threshold Th_v during successive samplings, the trajectory is changed. The magnitude of the difference in the velocity vector per unit of time among two successive measurements (the acceleration) is determined using velocity aspects from the NASA archive database that meets the next mentioned relationships:

$$\bar{v} = \overline{v_x} + \overline{v_y} + \overline{v_z} \tag{2}$$

$$a_i = \frac{\|\overline{\Delta v_i}\|}{\Delta t_i} = \frac{\|\overline{v_{i+1}} - \overline{v_i}\|}{t_{i+1}-t_i}, \qquad i = 1, 2, \cdots, N- \tag{3}$$

The velocity magnitude change could be calculated utilizing the next formula:

$$\|\overline{v_{i+1}} - \overline{v_i}\|^2 = \left(\Delta v_{x,i}\right)^2 + \left(\Delta v_{y,i}\right)^2 + \left(\Delta v_{z,i}\right)^2 \tag{4}$$

where $\Delta v_{x,i}$, $\Delta v_{y,i}$, $\Delta v_{z,i}$ represent the orthogonal velocity elements modification in the measurements interval i, and $i+1$. The scale of Cassini's acceleration could be observed on the left side of Fig. 14. It can be shown that the magnitude distribution of the acceleration is a power function. Acceleration refers to a shift of momentum, whether it is a change in speed, direction, or both.Where there is a variation in the velocity, the force of momentum is oriented

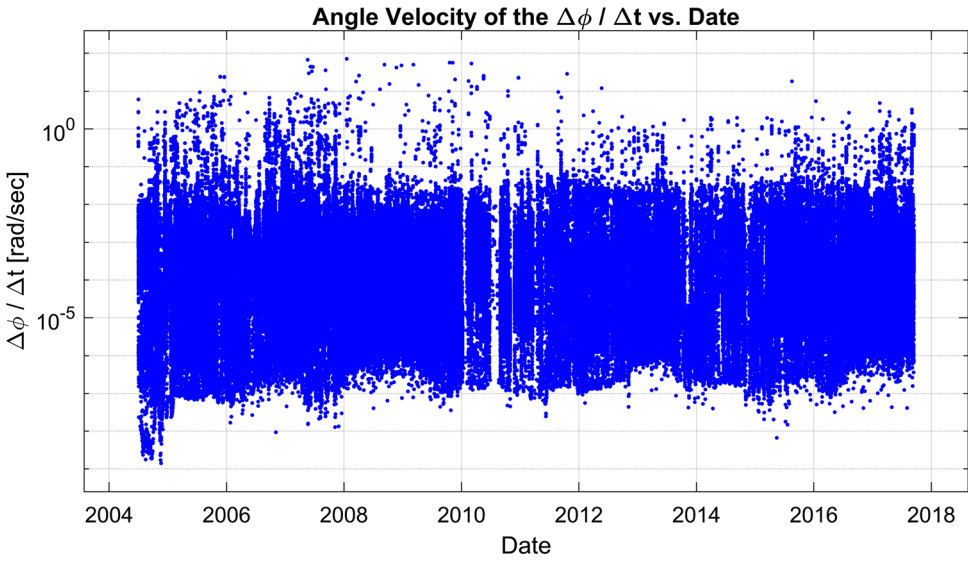

Fig. 13 Angle change per unit time of Cassini's successive velocity vectors (in the time interval after SOI till the mission ends)

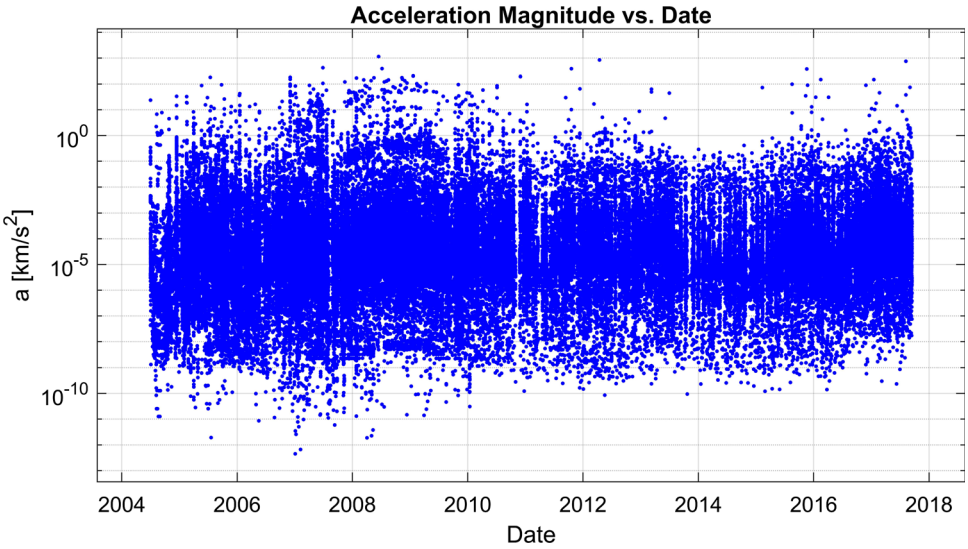

Fig. 14 Cassini's acceleration magnitude. The large amount of magnitudes are smaller than 1 km/s^2 (in the time interval after SOI till the mission ends)

ahead (in the case of deceleration) or behind (in the event of accretion in speed). While there is a shift in the course direction, the inertial force is directed, in this case, towards the left (for right-wing turn event) or towards the right-wing direction (in the situation of left rotation).

4.3 Recognition of complex events on the Cassini trajectory

In order to detect temporal semantics for complex accident detection, the primary objective behind the implementation of our classification is to use sensory information to recognize complex events. The complex events have only a single moment of observation at which they may take place; that is the pattern change moment. Let have trajectory shift indexes where particular events in a set I are given:

$$I_\phi = \left\{ 1 < i < N-1 \mid \frac{\Delta\phi_i}{\Delta t_i} \geq Th_\phi \right\} \tag{5}$$

$$I_a = \{ 1 < i < N-1 \mid a_i \geq Th_a \} \tag{6}$$

$$I = I_\phi \cup I_a \tag{7}$$

$$J = I_\phi \cap I_a \tag{8}$$

The indices I_ϕ and I_a reflect the modifications in the velocity direction among the examined NASA database, or the amplitude of the acceleration is higher than the correlated threshold point. The set J is used to concurrently sensitively consider the individual impact of the 2 criteria in the immediate previous two subsections. If the set J cardinality is strong, these two criteria are less dependent and may help recognize complex events across the trajectory. All of the sampling indexes observed by the envisaged complex event detector are included in the corresponding set I.

$$I = \{ i_1, i_2, \cdots, i_k \} \tag{9}$$

Following the SOI event in 2004, the spacecraft made numerous changes to its trajectory in response to orders from the Earth's supervisor squad. The amount of extreme events deemed Cassini trajectory modifications dependent on conditions (5) and (6) over the project's last 13.7 years is given by the cardinality k_I and k_J of the sets I and J, successively.

The number of trajectory modifications carried out should obviously be lower than the observations amount discussed in the section of (Cassini archive extraction and trajectories features), $M = 10,851$. According to Table 2, it was deemed 323 as the amount of executed maneuvers. We can calculate the operating point in three-dimensional space by leveraging the dependence of the amount of severe points within the threshold values Th_ϕ and Th_a throughout our framework. This dependence is represented as a surface plot in Fig. 15. The operating points are defined by red blister icons and are located at the extremes of the gradient's adjustment points. The working points are all in coordinate with extreme surfaces modification. To achieve the total amount of trajectory maneuvers, the threshold values are $(\mathrm{Th}_\phi, \mathrm{Th}_a) = (4.25\ \mathrm{rad}/s, 45.74\ \mathrm{km}/s^2)$.The cardinality of the I and J have been detected for these threshold levels to be $(k_I, k_J) = (287, 1)$. The left side of Fig. 16 shows a depiction of complex events observed in the set I_ϕ and I_a. There are 210 extreme events dependent on velocity vector alteration and 114 extreme events based on acceleration magnitude modification. The ensemble I, it is fair to say that set I_ϕ includes about twice as many serious events as the set I_a.

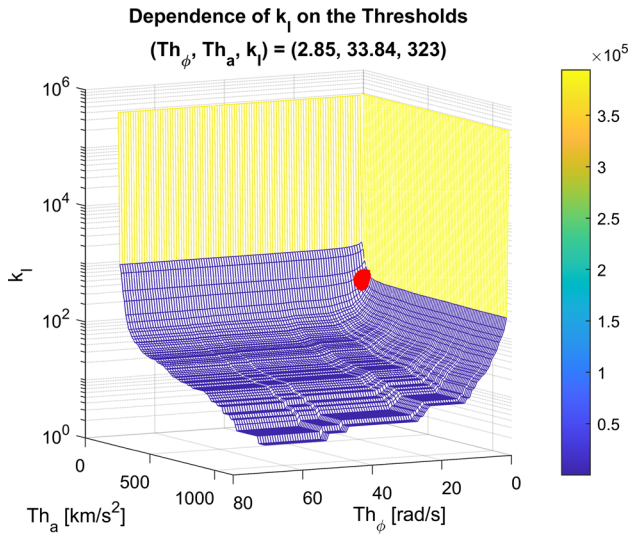

(a) The sets I cardinality

(b) The sets J cardinality

Fig. 15 The sets I (upper) and J (bottom) cardinality is based on the thresholds $Th_{\phi} and Th_{a}$

Diagram 17 shows Cassini's orbital coordinates during the trajectory modifications are displayed. The bulk of the trajectory maneuvers was completed during the Prime mission, with just a few changes made during the Solstice mission. To reach an identical spatial consensus between these two series, the combination of them both generates precisely 323 cases (unique extreme events) out of the trajectory adjustments. Consequently, we demonstrate how to detect these trajectory modifications by 3 types of RNNs.

In Fig. 17, the spatial positioning of Complex Event Detections (CEDs) of the planetary frame implies that the bulk of gambits was carried out during the first project phase (Prime). The star symbol represents the Sun, CED is given by plus sign, while a circle depicts the start of sampling, and the end of the sampling process is symbolized by cube shape.

5 Cassini trajectory modifications recognition by deep learning

The capacity of a model to recognize and recall trends within data to enhance the output, e.g., to use the current data to forecast events and overcome uncertainty, is referred to as appropriation with machine learning. Artificial intelligence is being used in various areas, including transportation, voice recognition, detection, etc. [23]. Since it can handle large databases, identify trends in image datasets, and determine spacecraft status, the technology is expected to be used to consolidate possible outer space research. Artificial intelligence has been a common tool for identifying the cause of a transition or a complicated incident. Because of machine learning, astronauts may be taught to navigate their vehicles in a limited time period to execute geometric maneuvers [24]. Accuracy would be demanded at greater and greater distances from Earth with the launch of increasingly complex and automatic-learning spacecraft. Orbit modification and automated-directed navigation could be included in the scope Centered on CED, we created RNN models and trained them to recognize those events. Exploiting the neural layers embeds vectors, especially with the ones that have a significant degree of dimensionality. The RNN layer accepts feedback from the embedding layer and provides a higher degree of abstraction to every data item.

The LSTM memory gating approach has converted the RNN into an efficient tool for encoding and capturing long-term dependence. The layered RNN solution could be thought of as an extension of the RNN paradigm with many hidden layers, each of which comprises many memory cells. More creative data assignments can be rendered open to other levels of RNN. We use the RNN layers method in which the performance of the previous LSTM layer is used as feedback for the next layer (check Fig. 18).

The periodic relation is a classic feature of RNN architecture, and it qualifies the RNN to upgrade or rejuvenate the current state based on former states in addition to the current input details [25].

5.1 RNNs framework for recognizing trajectory changes

The relationship between two or more concepts or events within the orbital entities will aid in the analysis of the impact on spacecraft trajectory, according to [26]. The accurate study of every frame requires the time relation for scientific findings. The suggested solution is an

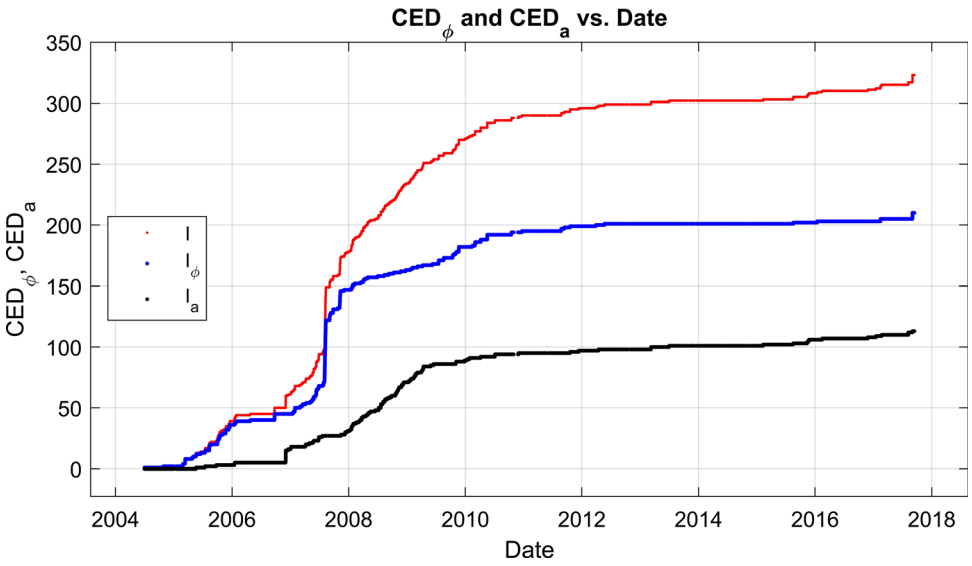

Fig. 16 Complex events observation (in the time interval SOI–end of mission)

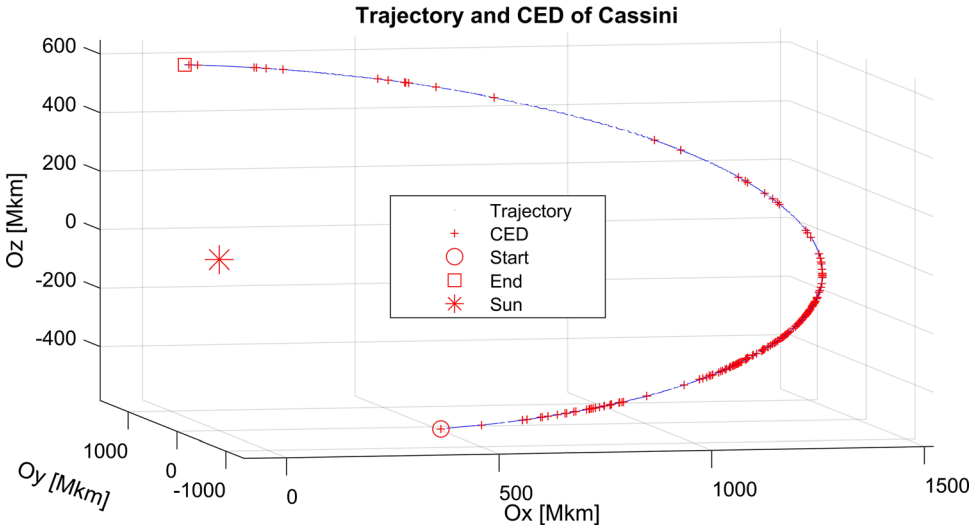

Fig. 17 The Cassini trajectory's complex events are plotted against the time (in the time interval SOI–end of mission)

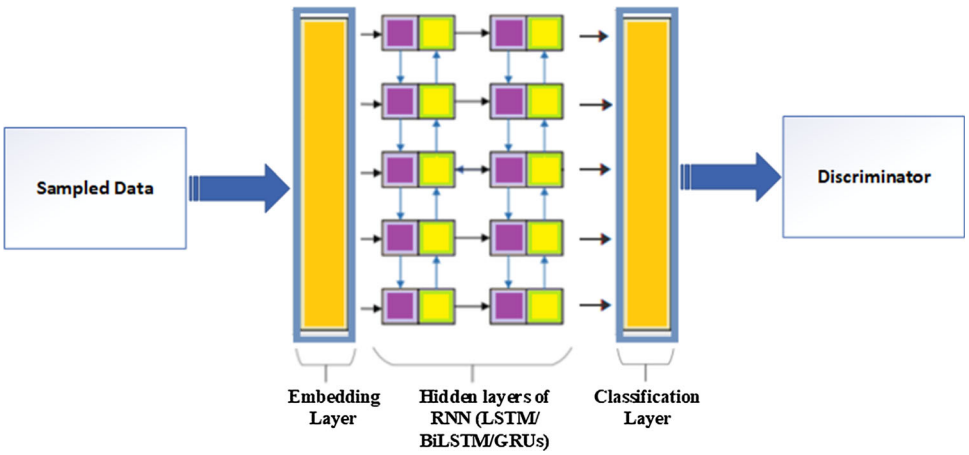

Fig. 18 RNNs generic utilized structure

amalgamated system that can determine trajectory changes among the C-H science missions. Trajectory analysis provides an ability not only to obtain knowledge about the movement of the spacecraft, but also to achieve a deeper analysis of movements depending on machine learning. Trajectory data were captured as input and evaluated in relation to the spacecraft velocity and the number of measurements that were taken during the mission. A series of sample ID $i \in \{1, \ldots, \ N-1=393,976\}$, is fed into the RNN framework, along with sampling periods $\Delta t_i = t_{i+1} - t_i$, adjustments to location coordinates $(\Delta x_i, \Delta y_i, \Delta z_i)$, and changes to velocity components $(\Delta v_{x,i}, \Delta v_{y,i}, \Delta v_{z,i})$ over the last 13.7 years of the mission examined data archive.The neural network's input is a7 x N matrix X that follows the formula:

$$X = [X_1, X_2, \cdots, X_{N-1}] \tag{10}$$

where the components of the column vectors X_i are as follows:

$$X_i = [\Delta t_i, \Delta x_i, \Delta y_i, \Delta z_i, \Delta v_{x,i}, \Delta v_{y,i}, \Delta v_{z,i}]^T \tag{11}$$

The $N-1$ sample data set is subdivided into object subsets. The first half is used for learning. The third and fourth quarters of data are used for validation and testing, respectively. In the RNN scheme, the samples are executed in a binary classification fashion and are divided into long sequences. It becomes apparent that the sequences of the examined multi-dimensional time series can be observed by the extreme events of the trajectory. The topology of the neural network is in Fig. 19.

The space probe made automatic modifications to hold the spacecraft on the complex helicoid explained previously in part 3. Due to the numerous science and astronomy goals of the mission, modification trajectory orders were often transmitted from the Planet of Earth by the technical control team. In order to recognize the memory tendencies to the analyzed data trajectory, we used RNNs with various parameters and layers. The outcome of the RNNs framework is a yes/no answer to the issue of whether or not the trajectory of Cassini has been changed.

The gradient threshold form is L2Norm, and the neural network training algorithm is ADAM. Table 3 lists the neural network's other parameters. Values of the table are default values of the Matlab procedures. It takes two categories to model the trajectory complex event. Each trajectory sample is classified Correct if the CED criteria (described in relations 6, 7) are satisfied; otherwise, it is classified as false. The confusion matrix serves to illustrate the classification model results and depicts the amount of correctly categorized samples in which classes [27].

Table 3 RNN parameter values

Option	Value
Gradient decay factor	0.9000
Squared gradient decay factor	0.9990
Initial learn rate	0.0200
Gradient threshold	1
Max epochs	100
Number of classes	2

The matrix accounts for the correspondence or disagreement between the goal values and the model predictions by considering the weighting factors. There are four variables in the confusion matrix, which are outlined below: True positive (TP) is the product of the algorithm correctly predicting a positive group.

At the point of diagnosis, the disorder is correctly defined. The result at which the model correctly forecasts the negative type is regarded as True Negative (TN). False Positive (FP) refers to when the algorithm forecasts a positive category incorrectly. Being not present has little impact on the condition's venue. A False Negative (FN) forecast is a category that is obtained when the model considers the state of being as being lower than it is. Such as the wrong prediction for the negative class, despite its presence, the condition is not found. Besides classification accuracy, a confusion matrix is often a possible intelligent option to better visualize the forecasts.

The cumulative number of data points in each cell is shown in the confusion matrix. The true class is represented by the confusion matrix rows, while the predicted class is represented by the columns. Correctly categorized observations are represented by diagonal cells, whereas

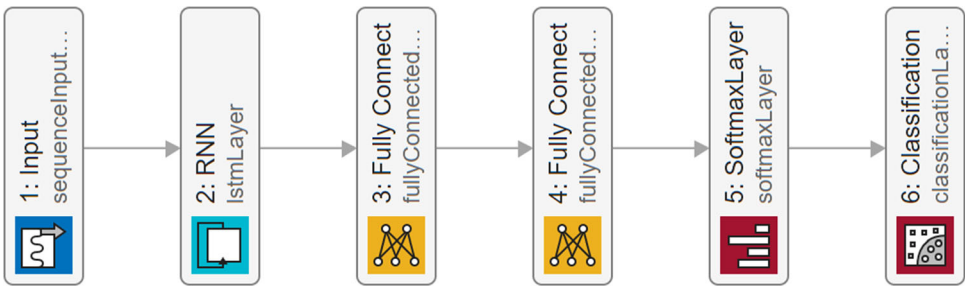

Fig. 19 Adopted RNN architecture. On layer two BiLSTM, GRU, and LSTM. Parameterized RNNs were used in various ways

misclassified observations are represented by off-diagonal cells. To every RNNs model, the Matthews correlation coefficient (MCC) is calculated by:

$$MCC = \frac{TP \cdot TN - FP \cdot FN}{\sqrt{(TP + FP) \cdot (TP + FN) \cdot (TN + FP) \cdot (TN + FN)}} \tag{12}$$

Criterion MCC relies heavily on the confusion matrix values. The numerator provides greater values as the TN and TP values get higher. It must be noted that since both TN and TP have big values, the numerator receives a large value. It could be shown that CMM has the highest possible value of 1 using Lagrange multipliers, owing to $(\mathrm{TP}, \mathrm{TN}, \mathrm{FP}, \mathrm{FN}) = (C/2,\ C/2, 0, 0)$ where C denotes the number of data items.

CMM, on the other hand, possesses the least value of -1 for $(\mathrm{TP}, \mathrm{TN}, \mathrm{FP}, \mathrm{FN}) = (0,\ 0, C/2, C/2)$. CMM is a metric for comparing and predicting tests and expected classes. It must be stated that if TP and TN are quite dissimilar and FN and FP are not near the value of 0, the metric CMM does not yield a large value. The confusion matrix is used to measure the F_1 score, but the True Negatives (TN) are overlooked. The F_1score is calculated as follows:

$$F_1 = \frac{2 \cdot TP}{2 \cdot TP + FN + FP} \tag{13}$$

F_1score is a test accuracy metric that can be explained as a weighted average of both precision and recall [28]. In order to measure the score, it considers both recall and precision. Precision is calculated by dividing the cardinality of true positive outcomes by the total amount of positive outcomes obtained via the learning process. The share of related samples which are correctly gained may be identified as the recall, which is the positive class precision. Precision/recall gives a valuable glimpse into the classifier's actions in the learning context [29]. The ideal F_1score value is 1, and the lowest score is 0. Precision and recall have the same proportional share as F_1 score. MCC is another reliable statistical assessment that yields a high score only if the prediction outcomes are successful in all of the 4 distinct classes of confusion matrix subsets where the negative/positive entities sizes are equal [30]. The MCC is unique for the purpose of binary classification if we have a binary indicator that can consistently differentiate all positive and all negative instances [31, 32].

When it comes to the precise significance of F_1score and MCC, a variety of scholars have varying opinions. Just about all reasonable output of standard measures reflects the ratio around the space dividing the amount of correctly labeled samples and the overall number of samples. (for example, (Wang et al., 2007)) [33]. MCC is distinguished from the F_1score by two main characteristics [34, 35]. Best of all,F_1varies for switching, but in the case where a negative class is renamed positive and vice versa, MCC never shifts. It has a second factor, the F_1, which is not connected to the amount of correctly classified negative samples.

6 Experimental results of the trajectory maneuvers detection

The research data sets in the Cassini mission were trained, validated, and tested with the portion of 50 %, 25 %, and 25 % respectively, on the last thirteen years and seven months of the project lifetime with 24 separate RNNs (to guarantee varied networks with various parameters). Eight of them are LSTM, eight are BiLSTM, and the rest are GRU networks.

As seen in Table 4, the varying input parameters (hidden units number, mini-batch size, layer three classes number, and layer four classes number), the detection accuracy of these networks, and the resulting learning time was also provided.

Figure 20 depicts a visual representation of the loss experienced through the learning phase. It is clear that the amount of hidden units on L2 has an effect on learning loss. The loss increases as the amount of hidden units decreases. The learning deficit is doubled when there are ten hidden units. An analogous feature is observed on the LSTM, BiLSTM, and GRU networks, but the last two seem to become over-learned after utilizing one hundred hidden units on the layer of L2.

We have trained the framework until it has completed 100 epochs and displayed the training loss values vs. the epochs number. Machine learning provides context for the data flowing out of a model simply by visualizing the model's performance. A learning curve is a graph that shows how well a model performs while learning new things over time or with training. These are often used in machine learning to diagnose systems that learn incrementally from a training dataset. After each iteration while training, the model may be assessed on the training dataset as well as on a hold-out validation dataset, and graphs of the measured performance can be produced to demonstrate learning curves for the model. It is possible to maximize the measure used to assess learning, which means that higher scores (bigger numbers) imply greater levels of learning. Classification accuracy is one such example. Better scores (lower numbers) imply greater learning, while a score of 0.0 implies that the training data was learned correctly and no errors were produced. It is more usual to employ a score that minimizes loss or error. A practical method to make sense of the data coming out of a machine learning model is to visualize its performance and make an educated choice about the adjustments that need

Table 4 The trajectory changes recognition accuracy among various RNNs

System	RNN type	Mini batch size	Hidden unites# on L2	Classes# on L3	Classes# on L4	Learning time [s]	Detection accuracy[%]
RNN_1	LSTM	1250	10	100	2	416.7	96.77
RNN_2	LSTM	1250	100	100	2	729.9	99.47
RNN_3	LSTM	2500	10	100	2	421.7	95.49
RNN_4	LSTM	2500	100	100	2	728.7	99.82
RNN_5	LSTM	5000	10	100	2	419.9	99.78
RNN_6	LSTM	5000	100	100	2	726.0	99.97
RNN_7	LSTM	10000	10	100	2	414.9	99.98
RNN_8	LSTM	10000	100	100	2	727.5	99.29
RNN_9	BiLSTM	1250	10	100	2	616.6	99.13
RNN_{10}	BiLSTM	1250	100	100	2	1292.6	99.98
RNN_{11}	BiLSTM	2500	10	100	2	615.3	95.15
RNN_{12}	BiLSTM	2500	100	100	2	1293.6	99.46
RNN_{13}	BiLSTM	5000	10	100	2	616.4	98.70
RNN_{14}	BiLSTM	5000	100	100	2	1293.4	99.89
RNN_{15}	BiLSTM	10000	10	100	2	617.6	99.90
RNN_{16}	BiLSTM	10000	100	100	2	1294.5	99.91
RNN_{17}	GRU	1250	10	100	2	407.9	99.21
RNN_{18}	GRU	1250	100	100	2	723.7	98.91
RNN_{19}	GRU	2500	10	100	2	409.4	98.90
RNN_{20}	GRU	2500	100	100	2	723.1	99.49
RNN_{21}	GRU	5000	10	100	2	410.2	96.55
RNN_{22}	GRU	5000	100	100	2	721.8	99.98
RNN_{23}	GRU	10000	10	100	2	411.9	99.57
RNN_{24}	GRU	10000	100	100	2	721.7	99.49

to be made to the model's parameters or hyperparameters. There may be a substantial difference in performance across models depending on how many nodes are in each layer and how many layers are in the network. Many hyperparameters can influence this, such as the neural network's node count per layer and the number of layers in the network. The improvement in the loss, as seen in Fig. 20, reflects the progress in training. The RNN's output improves incrementally as epochs advance successively. As the amount of epochs rises, the loss of training is reduced. As compared to other LSTM networks, RNN_7 LSTM has the lowest loss, i.e., the parameters used for the RNN models provide reliable results; in principle, the RNN may carry pertinent information throughout the sequence's processing. So even early knowledge may find its way into subsequent stages. A cyclical connection, which allows the RNN to upgrade the existing state depending on the previous states and current input data, is characteristic of the RNN architecture. RNN_{10} offers the highest outcomes in terms of losses among the other BiLSTM networks, and RNN_{22} GRU offers the highest outcomes in terms of losses among GRU networks. Also, it can be concluded that $RNN_{7,10,22}$ are providing the highest accuracy among all models. The ideal learning rate is unavoidably revealed to the data's lack of learned behavior, which is dependent on both the dataset and the model's design. The loss value shows how successfully or incompetently the model works during each learning iteration. The term "Epoch" refers to the process by which an entire dataset is transmitted forward and rearward across the neural network a single time. Adopting the confusion matrix is a significantly superior technique to assess a classifier's performance. It is a table that typically describes the effectiveness of a classification model, using a fixed set of data that has known actual values.

Classification tasks are often solved using the confusion matrix, which is a widely used tool. Use it to solve binary and multiclass classification issues, as well. visualization for the whole 24 RNNs is provided in Figure 21 as a logarithmic scale. It can be seen that the partial sum of the two smallest values (TN, FP) is always 21.

When it comes to describing the performance of classification algorithms, confusion matrix is the method to use. For example, if we have an uneven amount of

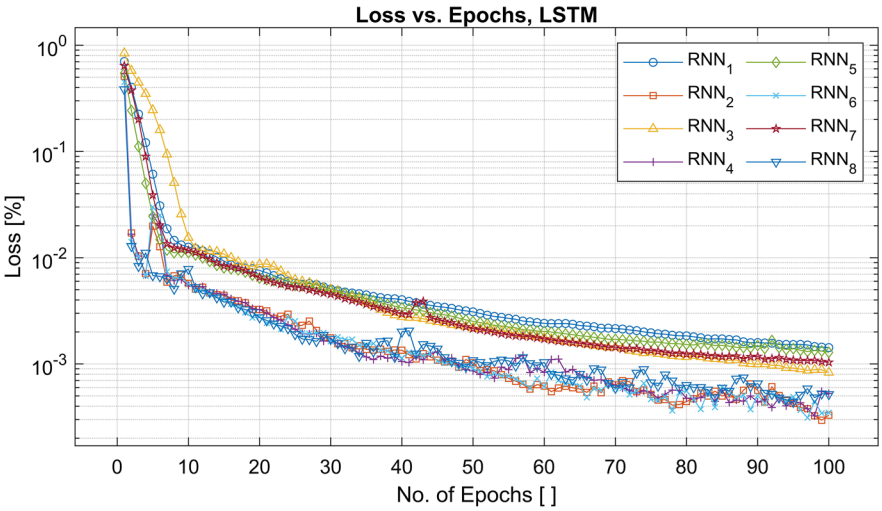

(a) RNNs LSTM loss

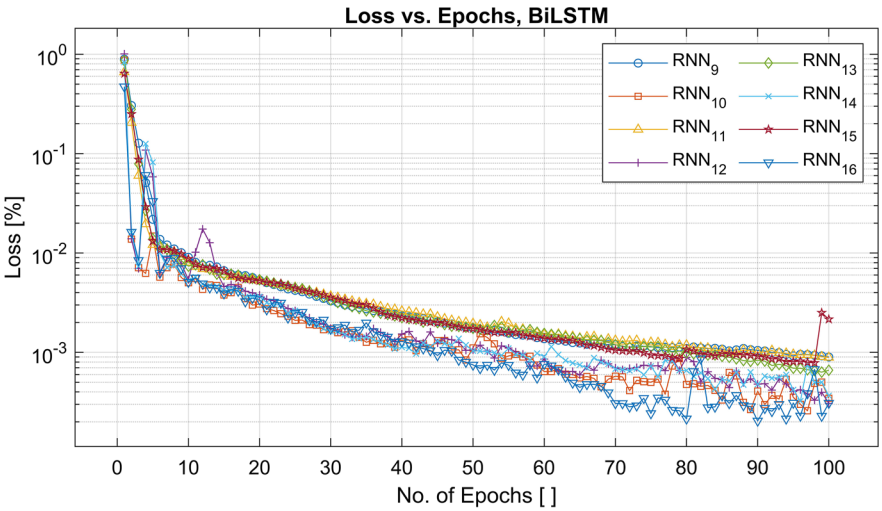

(b) RNNs BiLSTM loss

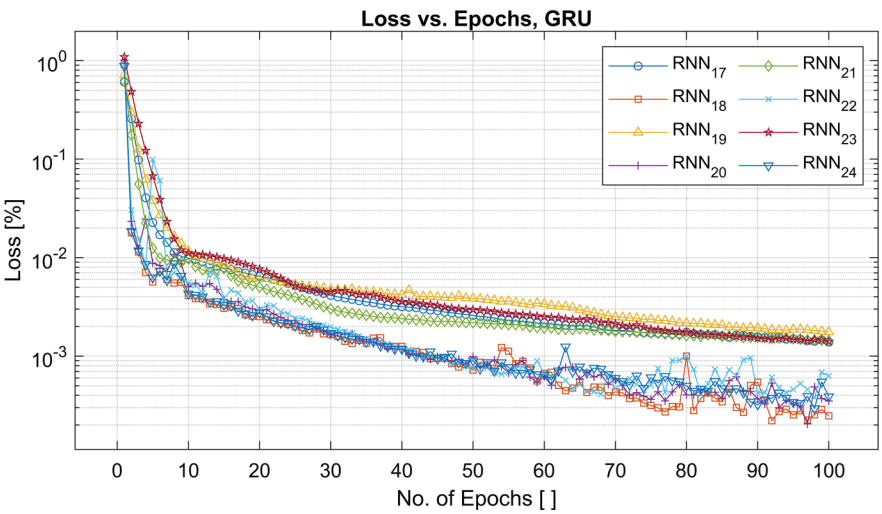

(c) RNNs GRU loss

Fig. 20 The minibatch learning loss reliance on RNNs epochs number for RNNs. Top: LSTM, middle: BiLSTM, bottom: GRU

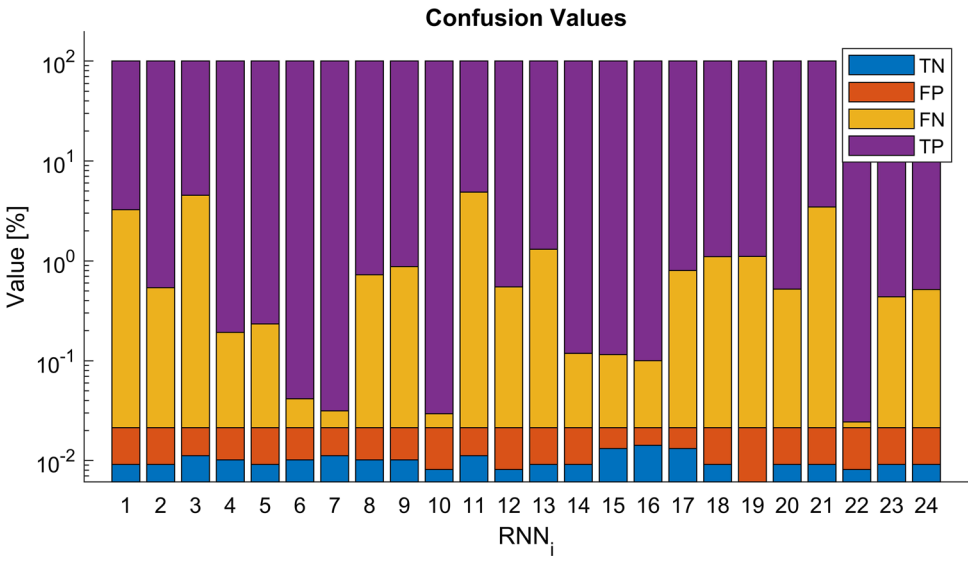

Fig. 21 Visualization of the 24 RNNs confusion values

observations at every class, or when we possess more than two classes in our dataset, just looking at classification accuracy alone may be deceiving. Making use of a confusion matrix may help us get a better understanding of what aspects of our classification model are correct and which kinds of mistakes it is making.This matrix is a representation of all of the predictions that have been made in comparison to the anticipated true values. Confusion matrices are useful for classifying issues since they show which predictions were incorrect and what kind of error was made. Each row and column in the confusion matrix is equal to the number of classes in the matrix.

Classification challenges are one of the specialties of neural network models that necessitate the use of machine learning techniques to learn how to give a class label to samples from the issue domain. Thus, neural network models are particularly well suited for classification tasks. It is evident on Fig. 22, that RNN_7 LSTM is offering the ideal accuracy when set side by side to other RNN network models, as it is achieving the highest scores and lowest learning time comparing to the other network's models. This is due to the related parameters, learning time, mini-batch size, and the number of hidden units.

The accuracy measure is used to calculate the model in an explainable way. The accuracy of the model is usually based on the values that are calculated by using the model parameters defined. It is known as the algorithm accuracy metric, reflecting the algorithm forecast in reference to the right data. Figure 22 depicts the relationship between accuracy and learning period with each of the RNNs studied. The RNN's accuracy was assessed by calculating loss across successive epochs. Most of the GRU networks

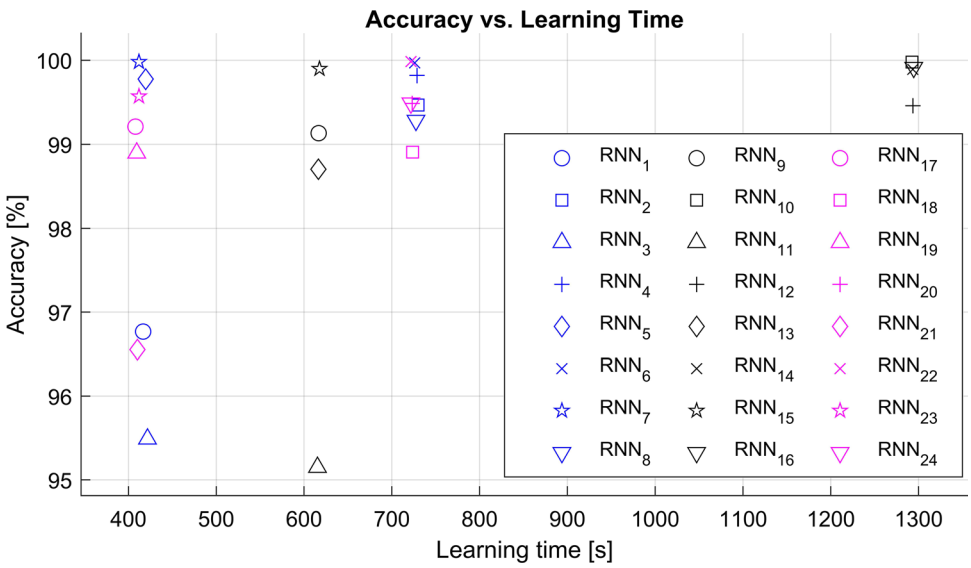

Fig. 22 Accuracy and learning speed of the RNNs as scatter plot (no symbol beneath the legend)

need less time to learn than BiLSTM and LSTM networks. Having different calculation formulas of performance metrics, we used multiple metrics to evaluate the relation between detection accuracy, MCC, and F_1 score of the analyzed data series. The graphic shows the relationship between accuracy and learning time after running the algorithm on the pre-selected set of models, the style is defined as a percentage pattern, and measured parameters are illustrated in the graphic. It is clear that RNN_7 is providing the highest accuracy and lowest learning time among the LSTM networks. While RNN_9 and RNN_{15} are having the lowest learning time and the highest accuracy among the BiLSTM networks. It can be noticed that RNN_{17} and RNN_{23} own the highest accuracy with the lowest learning time among the GRU Networks.

Table 5 displays the MCC and F_1 score of the corresponding neural networks. It attempts to contrast the F_1 score with the MCC, also demonstrate how the F_1 score might be beneficial for common classification tasks. A summary of the performances for the whole 24 RNNs network in terms of MCC is reported in Fig. 23. MCC is statistically elegant and all-encompassing in that the classifier's output is treated as a single variable, comparable to true labels.

When comparing two classes, the Matthews correlation coefficient provides a balanced measure of accuracy that may be utilized even when one class contains much more samples than the other. A coefficient of 1 represents flawless prediction, a value of 0 suggests random prediction, and a coefficient of -1 indicates inverse prediction.

Thus, the MCC seems to assist us to uncover the classifier's inefficiency in categorizing, particularly negative class data. Figure 24 indicates the dependence of the F_1 score parameter on an MCC. That makes it ideal for binary classification challenges. Within our case, MCC takes a range between 5% till 55% that's why the F_1 score is considered.

We often conceive of a connection between variables as a curve that fits the facts under consideration. Fit function curve with RNNs data points of MCC and F1 values is provided in Fig. 24, the fit curve appears as a black dotted line.

Approximation of the dependence of F_1 in function of MCC was found to be conformed to the following formula:

$$\log(\log(F_1)) \sim a{\cdot}MCC^b + c \cdot \mathrm{MCC}^d \tag{14}$$

where $(a, b, c, d) = (-0.227,\ -3.530,\ 1.526,\ 0.0002)$ with $R^2 = 0.896$. Neither F_1 or MCC are able to indicate exactly the accuracy of test results (see Table 5.). The following is a list of RNN indexes in tapering order for the MCC metric: 22, 7, 10, 6, 16, 15, 14, 4, 5, 17, 23, 24, 20, 2, 8, 12, 9, 18, 13, 3, 1, 11, 19, 21.

Through observing this outcome, it can be concluded that the optimal RNN to recognize the modification among Cassini trajectory is LSTM accompanied by 10 hidden units and a MiniBatch of 10000 and is able to model trajectory change behavior with 99.98% precision, with time equal to 6.9 minutes, also we can notice that GRU accompanied by 100 hidden units and a MiniBatch of 5000 and is able to model trajectory change behavior with 99.98% precision, with very little time fewer than 13.7 minutes on a desktop machine with 12 central processing cores, and 64 GB of RAM.

7 Conclusion

We rendered the beginning of an arrival point concerning Cassini trajectory modifications. As a result, we propose an innovative method for trajectory modification recognition based on a supervised methodology that makes use of the

Table 5 MCC and F_1 score of the analyzed RNNs

RNN	1	2	3	4	5	6	7	8
Type	LSTM							
MCC[%]	3.27	8.54	3.37	16.31	13.25	39.83	52.37	8.14
F_1[%]	98.36	99.73	97.69	99.91	99.89	99.98	99.99	99.64
RNN	9	10	11	12	13	14	15	16
Type	BiLSTM							
MCC[%]	7.37	43.63	3.23	7.52	5.37	19.13	27.52	31.82
F_1[%]	99.56	99.99	97.52	99.73	99.35	99.95	99.95	99.96
RNN	17	18	19	20	21	22	23	24
Type	GRU							
MCC[%]	10.06	5.87	3.86	8.69	3.16	52.63	9.53	8.73
F_1[%]	99.60	99.45	99.45	99.74	98.25	99.99	99.79	99.75

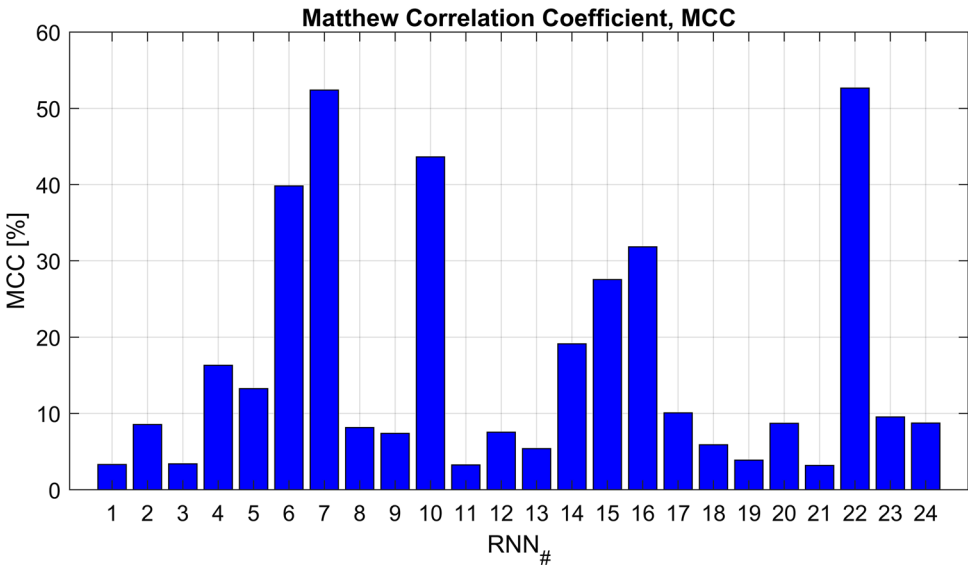

Fig. 23 Bar chart of the MCC values

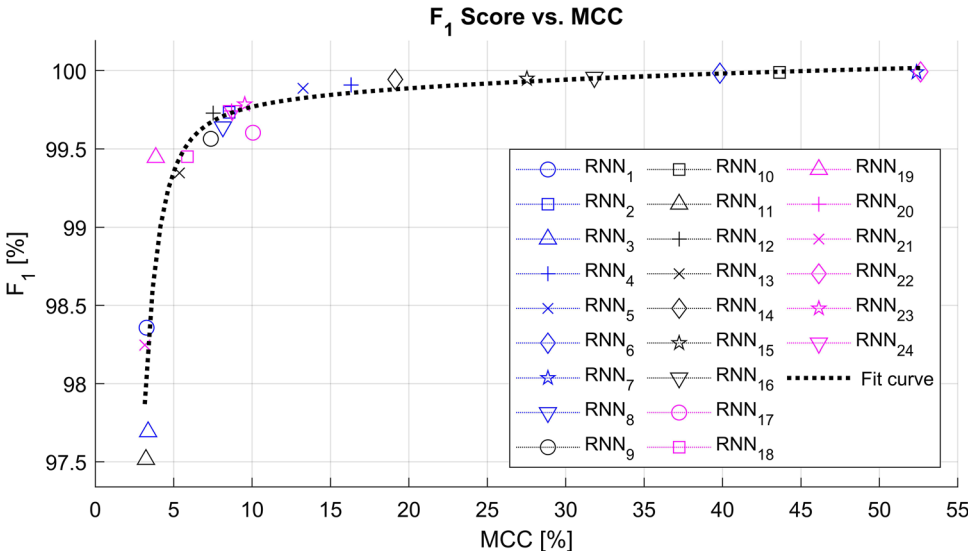

Fig. 24 Fit curve with RNNs data points of MCC and F_1 values

essential trajectory distinguishing attributes like the (velocity vector direction and magnitude). As far as we know, the recognition methods of Cassini trajectory modifications have been implemented via the LSTM/BiLSTM/GRU networks, which are the earliest research to identify the occurrences of adjustments in spacecraft routes. We demonstrate conclusively that our test study determines with a practical essence that the RNNS models with specific parameters are a reasonable option for forecasting Cassini trajectory modifications. Their use, combined with the addition of more stacked layers, results in a significant improvement in the detection process's efficiency. It is fair to say that the frameworks used here can easily be expanded to cover a wide range of scientific topics relevant to prediction. Using additional details, the given models make it possible to derive a correct inner-time dependence RNNs representation.

After analyzing the data, we discovered that MCC is better for binary classifications than F_1. The proposed recognition model is capable of identifying orbital changes with unprecedented precision, which is 99.98 percent via GRU and LSTM, which could be used for similar detection approaches on future space missions. Among our contributions, we develop a proper mapping between combining obtained spacecraft data and machine learning algorithms to uncover hidden insights automatically and without being instructed to do so. Finally, there is a major issue that needs to be addressed in our upcoming studies, which is the aspect of outliers. For dealing with this problem, our intelligent system must leverage unsupervised algorithms

to detect anomalies and outliers. In order to boost this, we will need a more evolved model.

Acknowledgements This paper was supported by the TKP2021-NKTA project of the University of Debrecen, Hungary, and by the QoS-HPC-IoT Laboratory.

Funding Open access funding provided by University of Debrecen.

Declarations

Conflict of interest The authors declare that they have no conflict of interest.

References

1. Salih FI, Ismail SA, Hamed MM, Yusop OM, Azmi A, Azmi NFM Data quality issues in big data: a review. In: International Conference of Reliable Information and Communication Technology, pp. 105–116 (2018). https://doi.org/10.1007/978-3-319-99007-1_11. Springer
2. ALDabbas A, Gal Z On the complex event identification based on cognitive classification process. In: 2019 10th IEEE International Conference on Cognitive Infocommunications (CogInfoCom), pp. 29–34 (2019). https://doi.org/10.1109/CogInfoCom47531.2019.9089989. IEEE
3. Dematteis G, Grafke T, Vanden-Eijnden E (2018) Rogue waves and large deviations in deep sea. Proc Natl Academy Sci 115(5):855–860. https://doi.org/10.1073/pnas.1710670115
4. Azmi NFM, Midi H, Ismail NF (2006) The performance of clustering approach with robust mm-estimator for multiple outlier detection in linear regression. J Teknologi. https://doi.org/10.11113/jt.v45.320
5. Meltzer M (2015) Building an international partnership and preventing mission cancellation. In: The Cassini-Huygens Visit to Saturn, Springer, pp. 27–46. https://doi.org/10.1007/978-3-319-07608-9_2
6. ALDabbas A, Gál Z (2019) Getting facts about interplanetary mission of cassini-huygens spacecraft. In: 10th Hungarian GIS Conference and Exhibition, Debrecen, Hungary
7. Szego K, Young DT, Barraclough B, Berthelier J-J, Coates AJ, McComas DJ, Crary FJ, Dougherty MK, Erdos G, Gurnett DA et al (2003) Cassini plasma spectrometer measurements of jovian bow shock structure. J Geophys Res: Space Phys. https://doi.org/10.1029/2002JA009517
8. Izzo D, Märtens M, Pan B (2019) A survey on artificial intelligence trends in spacecraft guidance dynamics and control. Astrodynamics 3(4):287–299. https://doi.org/10.1007/s42064-018-0053-6
9. Ahmarofi AA, Ramli R, Abidin NZ, Jamil JM, Shaharanee IN (2019) Variation on the number of hidden nodes through multilayer perceptron networks to predict the cycle time. J Inf Commun Technol 19(1), 1–19. https://doi.org/10.32890/jict2020.19.1.1
10. Al Nuaimi ZNAM, Abdullah R (2017) Neural network training using hybrid particlemove artificial bee colony algorithm for pattern classification. J Inf Commun Technol 16(2): 314–334. https://doi.org/10.32890/jict2017.16.2.6
11. Buffington B, Strange N, Ionasescu R (2005) Addition of a low altitude Tethys flyby to the nominal Cassini tour. Pasadena, CA: Jet Propulsion Laboratory, National Aeronautics and Space. https://trs.jpl.nasa.gov/handle/2014/39643
12. Stauch JR, Antreasian P, Bordi J, Criddle K, Ionasescu R, Jacobson R, Jones J, Meek MC, Roth D, Roundhill I (2005) Preparing for the Huygens Probe Mission, Cassini orbit determination results for the first and second targeted Titan encounters. Pasadena, CA: Jet Propulsion Laboratory, National Aeronautics and Space. http://hdl.handle.net/2014/39518
13. Bontemps L, Cao VL, McDermott J, Le-Khac N-A (2016) Collective anomaly detection based on long short-term memory recurrent neural networks. In: International Conference on Future Data and Security Engineering, Springer, pp. 141–152. https://doi.org/10.1007/978-3-319-48057-2_9
14. Liu J, Yu H, Cui S-h, Wang M, Li S-m (2016) Spacecraft trajectory forecasting method based on induced ordered information aggregation operator. In: 2016 IEEE Chinese Guidance, Navigation and Control Conference (CGNCC), pp. 1618–1621. https://doi.org/10.1109/cgncc.2016.7829032. IEEE
15. Spilker L, Edgington S (2019) Cassini-huygens: Recent science highlights and cassini mission archive. In: EPSC-DPS Joint Meeting 2019, vol. 2019, p. 2019. https://meetingorganizer.copernicus.org/EPSC-DPS2019/EPSC-DPS2019-978-1.pdf
16. Han P, Wang W, Shi Q, Yang J (2019) Real-time short-term trajectory prediction based on gru neural network. In: 2019 IEEE/AIAA 38th Digital Avionics Systems Conference (DASC), pp. 1–8. https://doi.org/10.1109/DASC43569.2019.9081618. IEEE
17. Silvestrini S, Lavagna MR (2020) Spacecraft formation relative trajectories identification for collision-free maneuvers using neural-reconstructed dynamics. In: AIAA Scitech 2020 Forum, p. 1918. https://doi.org/10.2514/6.2020-1918
18. Jarry G, Couellan N, Delahaye D (2019) On the use of generative adversarial networks for aircraft trajectory generation and atypical approach detection, 1918 (227–234). https://doi.org/10.1007/978-981-33-4669-7_13
19. Fritz S, Turkoglu K (2016) Optimal trajectory determination and mission design for asteroid/deep space exploration via multi-body gravity assist maneuvers. In: 2016 IEEE Aerospace Conference, pp. 1–9. https://doi.org/10.1155/2017/6801023. IEEE
20. Antreasian P, Ardalan S, Bordi J, Criddle K, Ionasescu R, Jacobson R, Jones J, MacKenzie R, Parcher D, Pelletier F, et al (2008) Cassini orbit determination results january 2006-end of prime mission. In: AIAA/AAS Astrodynamics Specialist Conference and Exhibit, p. 6747. https://doi.org/10.2514/6.2008-6747
21. Aeronautics, N of the USA., S.A (2022) Cassini ISS Online Data Volumes, Imaging Science Subsystem (ISS), Saturn EDR Data Sets, Vol. 1 – 116. Figshare https://pds-imaging.jpl.nasa.gov/volumes/iss.html
22. Buffington B (2020) Designing the Cassini solstice mission trajectory: ASK magazine, 15. https://appel.nasa.gov/wpcontent/uploads/2013 /04/513854main_ASK_41s_designing.pdf
23. Hegde J, Rokseth B (2020) Applications of machine learning methods for engineering risk assessment-a review. Saf Sci. https://doi.org/10.1016/j.ssci.2019.09.015

24. Sharma S, D'Amico S (2019) Pose estimation for non-cooperative rendezvous using neural networks. arXiv preprint arXiv:1906.09868, 1–12. https://doi.org/10.1109/AERO.2018.8396425
25. Yu Y, Si X, Hu C, Zhang J (2019) A review of recurrent neural networks: Lstm cells and network architectures. Neural Comput. 31(7):1235–1270. https://doi.org/10.1162/neco_a_01199
26. ALDabbas A, Gál Z (2019) Complex event processing based analysis of cassini–huygens interplanetary dataset. In: International Conference on Information, Communication and Computing Technology, pp. 51–66. https://doi.org/10.1007/978-3-030-38501-9_5. Springer
27. Taylor W, Shah SA, Dashtipour K, Zahid A, Abbasi QH, Imran MA (2020) An intelligent non-invasive real-time human activity recognition system for next-generation healthcare. Sensors 20(9):2653. https://doi.org/10.3390/s20092653
28. Sokolova M, Lapalme G (2009) A systematic analysis of performance measures for classification tasks. Inf Proc Manag 45(4):427–437. https://doi.org/10.1016/j.ipm.2009.03.002
29. Buckland M, Gey F (1994) The relationship between recall and precision. J Am Soc Inf Sci 45(1):12–19
30. Chicco D, Jurman G (2020) The advantages of the matthews correlation coefficient (mcc) over f1 score and accuracy in binary classification evaluation. BMC Gen 21(1):1–13. https://doi.org/10.1186/s12864-019-6413-7
31. Jurman G, Riccadonna S, Furlanello C (2012) A comparison of mcc and cen error measures in multi-class prediction e41882. https://doi.org/10.1371/journal.pone.0041882
32. Chicco D (2017) Ten quick tips for machine learning in computational biology. BioData Min 10(1):1–17. https://doi.org/10.1186/s13040-017-0155-3
33. Wang L, Chu F, Xie W (2007) Accurate cancer classification using expressions of very few genes. IEEE/ACM Trans Comput Biol Bioinf 4(1):40–53. https://doi.org/10.1109/TCBB.2007.1006
34. Sasaki Y, et al (2007) The truth of the f-measure. URL: https://www. cs. odu. edu/~ mukka/cs795sum09dm/Lecturenotes/Day3/F-measure-YS-26Oct07. pdf [Accessed 2021-05-26] 1(5), 1–5 (2007)
35. Powers DM (2015) What the f-measure doesn't measure: Features, flaws, fallacies and fixes. CoRR abs/1503.06410. https://doi.org/10.13140/RG.2.2.23168.79361